Journal of Power Sources 196 (2011) 6092–6098

Contents lists available at ScienceDirect

Journal of Power Sources

journal homepage: www.elsevier.com/locate/jpowsour

Evaluation of the catalytic activity of Pd–Ag alloys on ethanol oxidation and oxygen reduction reactions in alkaline medium

M.C. Oliveira*, R. Rego, L.S. Fernandes, P.B. Tavares

CQ-VR, Centro de Química - Vila Real, Department of Chemistry, University of Trás-os-Montes e Alto Douro, Apartado 1013, 5001-801 Vila Real, Portugal

ARTICLE INFO

Article history:
Received 17 November 2010
Received in revised form 4 March 2011
Accepted 27 March 2011
Available online 6 April 2011

Keywords:
Ethanol oxidation reaction (EOR)
Pd–Ag
Pd alloy
Oxygen reduction reaction (ORR)
Direct ethanol fuel cell (DEFC)
Alkaline medium

ABSTRACT

Pd–Ag alloys containing different amounts of Ag (8, 21 and 34 at.%) were prepared in order to evaluate their catalytic activity towards the ethanol oxidation (EOR) and oxygen reduction (ORR) reactions. A sequential electroless deposition of Ag and Pd on a stainless steel disc, followed by annealing at 650 °C under Ar stream, was used as the alloy electrode deposition process.

From half-cell measurements in a 1.0 M NaOH electrolyte at ≅20 °C, it was found that alloying Pd with Ag leads to an increases of the ORR and EOR kinetics, relative to Pd. Among the alloys under study, the 21 at.% Ag content alloy presents the highest catalytic activity for the EOR and the lowest Ag content alloy (8 at.% Ag) shows the highest ORR activity. Moreover, it was found that the selectivity of Pd–Ag alloys towards ORR is sustained when ethanol is present in the electrolyte.

1. Introduction

A new era of research on direct alcohol fuel cells (DAFCs) is emerging with the recent development of alkaline membranes [1]. For decades, the development of new electrode materials for polymer electrolyte membrane fuel cells concerned almost exclusively the acid medium. However, since the appearance of alkaline membranes electrocatalytic studies, including ethanol oxidation reaction (EOR) and oxygen reduction reaction (ORR), turned towards the alkaline medium [2]. One of the main advantages of alkaline medium comes from the fact that the electrode reaction kinetics in this medium is higher than in the acid medium, enabling the use of Pt-free catalysts. Moreover, the alkaline media provides a less corrosive environment to the electrodes.

Recent studies have shown that Pd-based catalysts are very attractive for both EOR [3,4] and ORR [5,6] in alkaline medium, representing an important alternative to Pt-based catalysts for direct ethanol alkaline fuel cells (DEAFCs).

Concerning the anode side reaction of DEAFC, some effort has been devoted to employ Pd-alloys looking for a synergetic effect between Pd and the alloying element. So far, such an effect has been observed in the alkaline medium on Pd–Au [7], Pd–Pt [8], Pd–Sn [9], Pd–Pb [10] and Pd–Ni [11] alloys. Recently, Nguyen et al. [12] showed that Pd–Ag/C also presents a good catalytic activity towards EOR, but the exact nominal composition of the Pd alloy was not determined.

Regarding the cathode side reaction, Pd-based catalysts have shown a surprisingly high ORR activity, particularly in the alkaline medium, with an ORR activity close to that of Pt. The use of Pd alloys catalysts for the ORR came out with the first publication by Savadogo group in 2004, which addressed the Pd–Co use in the acid medium [13]. Since then, a wide range of Pd alloys have been investigated, although the number of works reported for the alkaline medium is still very low, confined to Pd–Ni [14], Cu–Pd [15], Fe–Pd [16] and Pd–Sn [17]. Recently, it has been shown that, in this medium, the ORR activity of silver nanoparticles coated with Pd is improved by a factor of two compared to commercial Pt [18]. Although palladium and silver display individually a high electrocatalytic activity towards the oxygen reduction reaction (ORR) in the alkaline medium, the activity of Pd–Ag alloys towards ORR has never been studied. Contrasting to other Pd alloys, Pd–Ag alloys are known to form a homogenous solid solution at all compositions, which makes them very attractive.

In this work, Pd–Ag alloys containing different amounts of Ag were prepared and their intrinsic catalytic activities towards EOR and ORR in alkaline media were evaluated from half-cell measurements. In order to simplify the experimental procedure, the Pd–Ag alloys were prepared as thin films deposited on a stainless steel substrate.

* Corresponding author. Tel.: +351 259350286; fax: +351 259350480.
E-mail address: mcris@utad.pt (M.C. Oliveira).

0378-7753/$ – see front matter © 2011 Elsevier B.V. All rights reserved.
doi:10.1016/j.jpowsour.2011.03.062

Table 1
Composition of Pd and Ag plating solutions.

Pd–Ag alloy (at.% Ag)	Ag plating					Pd plating				
	Ag^{+} (mM)	EDTA (M)	N_2H_4 (mM)	NH_4OH (M)	t (min)	Pd^{2+} (mM)	EDTA (M)	N_2H_4 (mM)	NH_4OH (M)	t (min)
0	–	–	–	–	–	28.0	0.10	30	4.0	210
8	3.0	0.11	12	3.5	60			30		180
21			6.0		210			27		210
34	17.5		10.0		210			27		180
100	3.0		6.0		180	–	–	–	–	–

2. Experimental

2.1. Preparation of Pd–Ag films

Pd alloy films were deposited on stainless steel discs (⌀ = 6 mm, AISI 316L) previously polished with emery paper (1000 grade), washed in a sonicated bath and annealed at 600 °C in air for 5 h. This procedure was important in order to form an oxide film which works as an intermetallic diffusion barrier, avoiding the formation of undesirable alloy phases between substrate components (Fe, Cr or Ni) and the Pd or Ag layer [19,20]. After this procedure the substrates were submitted to sensitizing/activation steps by successive dipping in $SnCl_2$ (1.0 g l^{-1} in 0.20 M HCl) and $PdCl_2$ (0.1 g l^{-1} in 0.20 M HCl) with intermediate de-ionized water rinsing. This sequence was repeated four times. These sensibilization/activation steps were necessary to seed the oxidized stainless steel substrate with catalytic nucleus, as it is not catalytic for the electroless deposition. Sequential metal plating was performed on the oxidized/sensitized-activated substrate. Silver was first deposited at 60 °C, followed by palladium deposition at room temperature. The plating conditions for palladium and silver electroless deposition are given in Table 1 [21,22]. For both palladium and silver, the deposition was performed in 10 ml of plating solution under stirring. After the two layers deposition, the prepared films were rinsed with deionised water, dried in an oven at 40 °C for 24 h and finally annealed in argon atmosphere at 650 °C for 6 h. This temperature is above the Tamman temperature for either Ag (344 °C) and Pd (640 °C), but below Fe_2O_3 (780 °C), therefore is sufficiently high to form the Pd–Ag alloy on the oxidized substrate.

2.2. Electrochemical and physical characterization of Pd–Ag films

Structural analysis of the films was carried out by X-ray diffraction in a PAN'Analytical X'Pert Pro diffractometer, equipped with a X'Celerator detector and secondary monochromator, using CuK_α radiation. To increase the signal from the films the spectra acquisition was performed at a constant $\omega = 10°$ (incident angle on the sample) and scanning the detector on 2θ. The analyses of the diffraction spectra were performed using the Rietveld method with PowderCell software. On the SEM/EDS analysis a FEI Quanta 400 microscope was employed. The alloy composition, obtained from EDS analysis was expressed in atomic percentage of silver and represents an average value from the analysis of five different points of the surface sample.

On the EOR study, the voltammetric experiments were performed by scanning the potential in the anodic direction at a scan rate of 20 mV s^{-1}. The electrolyte aqueous solutions, 1.0 M NaOH + 1.0 M EtOH, were deaerated and an oxygen-free nitrogen atmosphere was kept in the cell during the measurements. On the ORR study, the potential was scanned in the cathodic direction, at a scan rate of 5 mV s^{-1} in a O_2-saturated 1.0 M NaOH aqueous solution. The O_2 gas was bubbled into the cell for 40 min to obtain a O_2-saturated solution at atmospheric pressure. Electrochemical experiments were performed in one-compartment cell with a Pt flag and a saturated calomel electrode (to which the potential is referred) as the counter and reference electrode, respectively. The stainless steel disk with a Pd–Ag film deposited on the top (geometric area of 0.196 cm^2) was used as the working electrode. The film contact with the solution was assured by the dipping technique [23]. The electrode potential was controlled by an Autolab potentiostat model 100. All electrochemical experiments were performed at room temperature (20 ± 1 °C). The reproducibility of the presented data was appraised from at least three replicas.

3. Results and discussion

3.1. Physical characterization

A typical XRD pattern of Pd–Ag film obtained before annealing is shown in Fig. 1. The diffraction peaks of (1 1 1), (2 0 0), (2 2 0) and (3 1 1) Pd planes appeared at $2\theta = 40.18°$, 46.80°, 68.35° and 82.11°, respectively, while those of Ag appeared at $2\theta = 38.1°$, 44.4° and 64.5° and 77.4°. After annealing, pure Pd and Ag phases disappeared to form a fcc Pd–Ag alloy phase whose diffraction peaks appear between those of Pd and Ag. A single phase was present on all samples, excepting on the alloy with the highest Ag content. A detailed analysis of the X-ray diffractogram of this sample using Rietveld refinement (PowderCell software) allowed concluding the formation of a three phase mixture containing: (i) 71.3 at.% of $Pd_{0.72}Ag_{0.28}$; (ii) 22.5 at.% of $Pd_{0.47}Ag_{0.53}$; (iii) 6.2 at.% of Pd (see supporting information). Taking into account the above mentioned phases and their respective atomic percentage, an average of 32 at.% Ag is obtained, close to the average chemical composition provided by the EDS analysis, 34 at.% Ag. The EDS analysis was performed at five different regions of 1 mm × 1 mm on the surface sample.

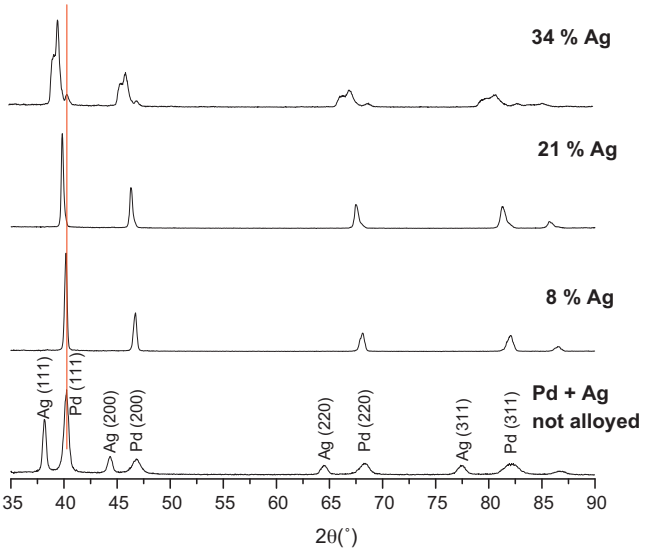

Fig. 1. X-ray diffraction patterns of Pd + Ag films (before annealing) and Pd–Ag alloys films with different Ag contents.

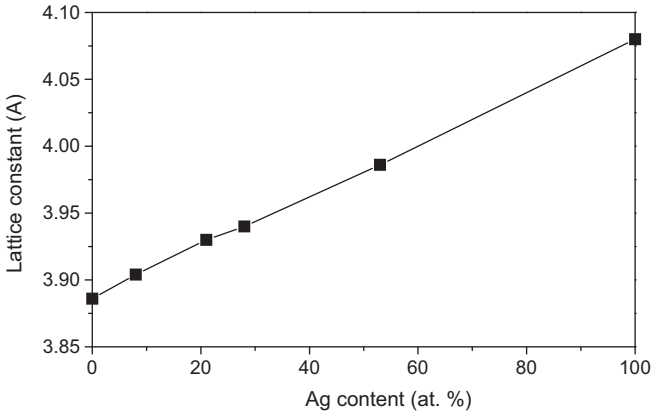

Fig. 2. Lattice constant of Pd–Ag alloy *vs* Ag content (at.%) in the alloy.

On changing the Pd–Ag alloy composition a shift in the diffraction line positions of the XRD pattern was observed, in accordance with the change in the lattice parameter. This shift varies continuously from pure Ag to pure Pd (Fig. 2) as expected for two metals that are completely soluble in the solid state.

The Pd–Ag alloys films were also characterized by scanning electron microscopy (SEM), Fig. 3. The SEM images show that the morphology of Pd–Ag alloys depends on the Ag content. On increasing the Ag content from 8 at.% to 34 at.%, the morphology of the deposit changes from a cluster-like deposit comprised of small discrete particles to a sintering-like deposit.

Regarding the observed dependence of the surface morphology on the alloys composition, it cannot be ruled out the hypothesis that the different surface morphology could also affect, in some extent, the catalytic activity of the Pd–Ag alloys towards the EOR and ORR. In the present work these two effects, morphology and composition, cannot be unequivocally separated.

From the cross-section view, the film appears dense and homogeneous over the substrate, although some little holes trapped along the film appear, as predicted from the top view. The alloys thickness, estimated from the cross-sectional SEM image of replicas (films prepared in the same experimental conditions), was in the range of 3–6 μm. Due to the low stability of the electroless plating solutions it was difficult to reproduce the film thickness.

3.2. Electrochemical characterization in 1.0 M NaOH

The cyclic voltammogram behavior of Pd–Ag alloys was preliminarily investigated in the 1.0 M NaOH aqueous solution. The obtained voltammograms are illustrated in Fig. 4a and, for comparison, the voltammogram of bulk Pd is also shown. Comparing the voltammograms obtained for the various compositions of Pd–Ag, it is concluded that they broadly maintain the Pd voltammetric features, i.e. formation and reduction of Pd oxide and absorption/desorption of hydrogen. However, it should be noted that on the richest Ag alloy, no H desorption peak is observed and a small reduction peak located at −0.065 V is detected. The latter is ascribed to AgOH or Ag_2O reduction which is indicative that a small amount of silver is present on the electrode surface, probably due to surface segregation phenomena, a common phenomenon in alloy systems [24]. The non detection of the H desorption peak reveals that the high Ag content alloy prevents hydrogen absorption, most likely due to the very low H diffusivity at such conditions, as predicted by the effect of the silver content on the H diffusivity in the Pd alloy [25].

Another interesting feature concerns the Pd oxide reduction peak potential which shifts towards more positive potentials as the Ag content of the alloy decreases. This behavior, more evident when the voltammograms are recorded in a narrower potential range (Fig. 4b), seems to reflect the weakness of interaction between the oxygenated species (OH_{ads}) and the substrate, indicating that the alloy displaying the lower ability for the OH adsorption and oxide formation is the lowest Ag content alloy (8 at.%).

Making use of the voltammetric profile resemblance between Pd and Pd–Ag alloys and the absence (or negligible amount) of Ag on the surface, the electrochemical active surface area (EASA) was evaluated using the approach developed by Correia et al. [26] and regularly applied to other Pd alloys [27]. This method relies on the evaluation of the charge consumed in the formation of a PdO monolayer which is depicted from a plot that relates the reduction charge of this oxide with increasing anodic inversion potentials. The surface roughness obtained allowed concluding that it increases (2.1, 3.5, and 5.8) on going from 8% to 34 at.% Ag.

3.3. Ethanol oxidation reaction

The linear voltammograms, based on the electrochemical active surface area (EASA), of pure Pd and Pd–Ag alloys in 1.0 M EtOH + 1.0 M NaOH solution, are illustrated in Fig. 5 and the cor-

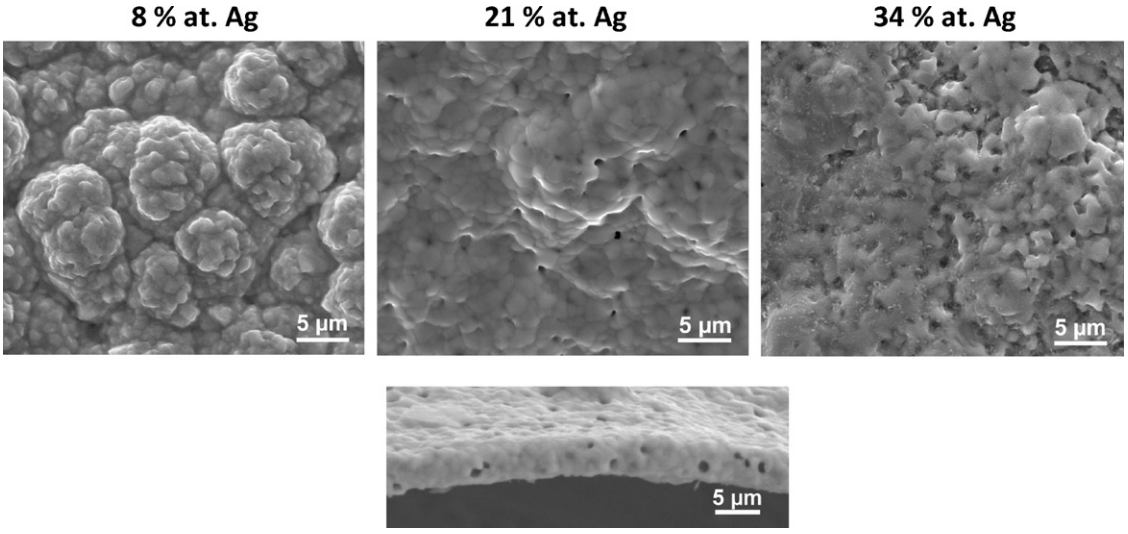

Fig. 3. SEM images of Pd–Ag alloy films with different contents of Ag (8, 21 and 34 at.% Ag) and cross-section view of a typical alloy film (containing 21 at.% Ag).

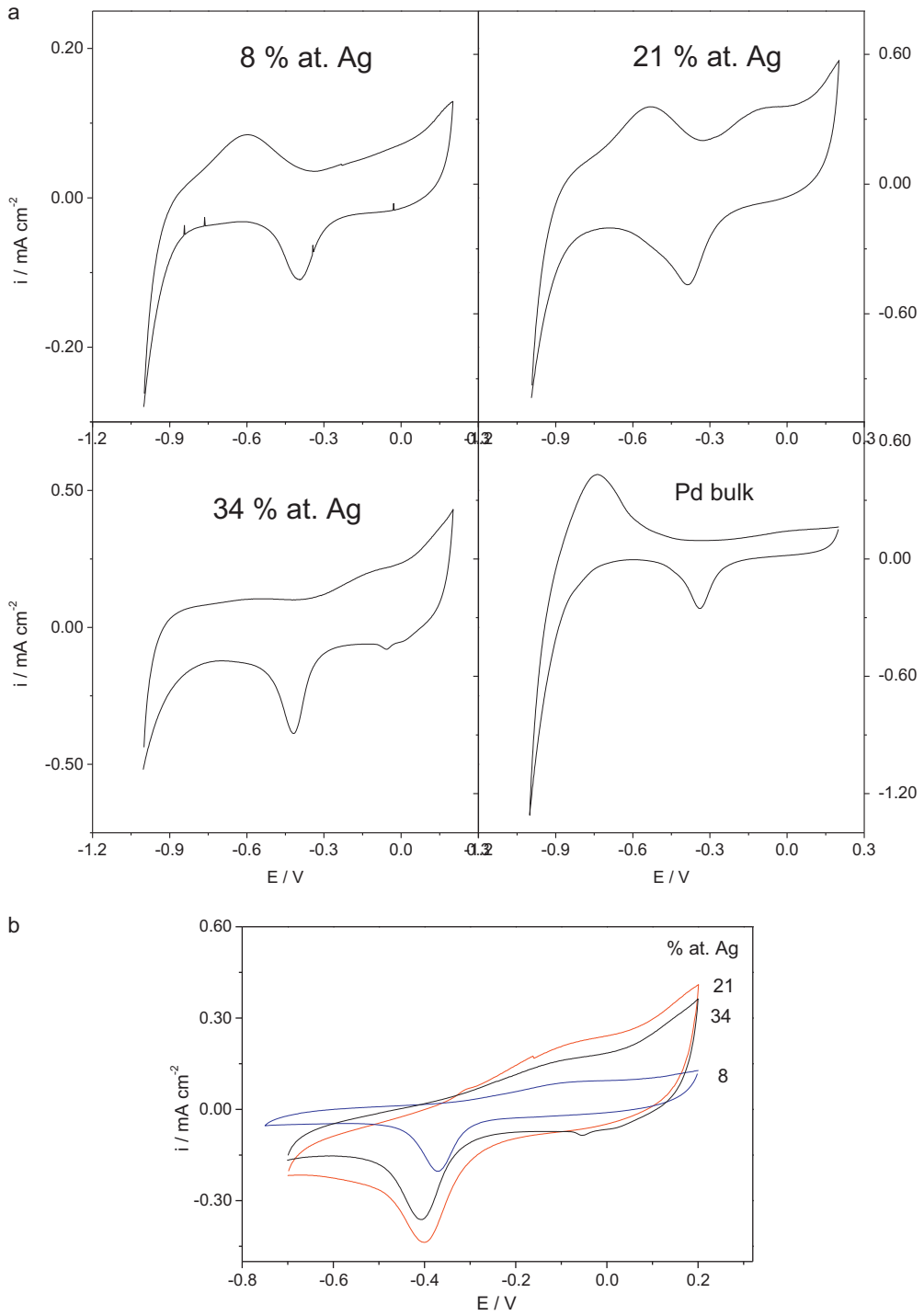

Fig. 4. Cyclic voltammograms of Pd–Ag alloy films (8, 21 and 34 at.% Ag) in 1.0 M NaOH solution in (a) a potential range containing the H-region and (b) in a narrower potential range. The current was normalized to the geometric surface area. $\upsilon = 20\ mV\ s^{-1}$.

Table 2
Voltammetric parameters for the ethanol oxidation on Pd–Ag alloys and Pd bulk in 1.0 M NaOH + 1.0 M EtOH.

Electrocatalyst		Onset potential for EOR (mV)	Potential at peak maximum (mV)	Peak current density ($mA\ cm^{-2}$)
Pd–Ag	8 at.% Ag	≅−0.80	−302	3.46
	21 at.% Ag	≅−0.80	−244	5.17
	34 at.% Ag	≅−0.80	−291	2.44
Pd		−0.70	−325	1.12

Table 3
Electrode kinetics parameters for the ORR on Pd–Ag alloys and Pd bulk in 1.0 M NaOH.

Electrocatalyst		Onset potential for ORR (mV)	i at −0.25 V (mA cm^{-2})	$-b$ (mV dec^{-1})	
				High overpotential	Low overpotential
Pd–Ag	8 at.% Ag	−150	−0.480	163	44
	21 at.% Ag	−150	−0.315	222	62
	34 at.% Ag	−160	−0.112	211	59

responding onset oxidation potential (E_{onset}), peak current density (I_p) and peak potential (E_p) are shown in Table 2. To compare their intrinsic catalytic activity towards the EOR the current was normalized to EASA.

At the beginning of the anodic scan, a small steady reduction current is detected, most probably due to residual oxygen in solution. This effect is more evident on the 8% Ag alloy, which as will be seen in Section 3.4, exhibits the highest ability for the oxygen reduction reaction. Due to this behavior, an accurate E_{onset} determination on the three Pd–Ag alloys is difficult. Even so, we can conclude that it is clearly more negative (approximately 100 mV) than on bare Pd, which is indicative that the Pd–Ag alloys are more active towards the EOR than bare Pd.

The voltammograms displayed in Fig. 5 reveal that the catalytic activity towards EOR is sensitive to the Ag content of the alloy and that the Pd–Ag alloy containing 21 at.% Ag exhibits the highest activity. Its peak current density is not much different from the one obtained on Pd–Ag/C [12]. These preliminary results point out for a "volcano" type relationship between the composition and catalytic activity of Pd–Ag alloys, resembling the behavior found for Pt–Ru [28].

It is interesting to note that the peak potential also changes with the alloy composition. The alloy displaying the more negative peak potential is the one that revealed the lowest ability for the oxide formation (8 at.% Ag alloy), indicating that the peak profile in the anodic scan cannot be solely rationalized in terms of blockage of ethanol adsorption by surface oxides [29], but other(s) phenomena must be also responsible for the surface blockage and consequently for the current drop.

In order to assess this hypothesis and evaluate the catalytic activity of the Pd–Ag alloys in steady state conditions, the current–time response was monitored during 40 min after application of a potential out of the oxide region (−0.4 V), Fig. 6. The obtained results support the conclusion that the 21 at.% Ag alloys is the highest active alloy for the EOR. Moreover, the fastest current decay observed on the 8 at.% Ag alloy is consistent with its surface

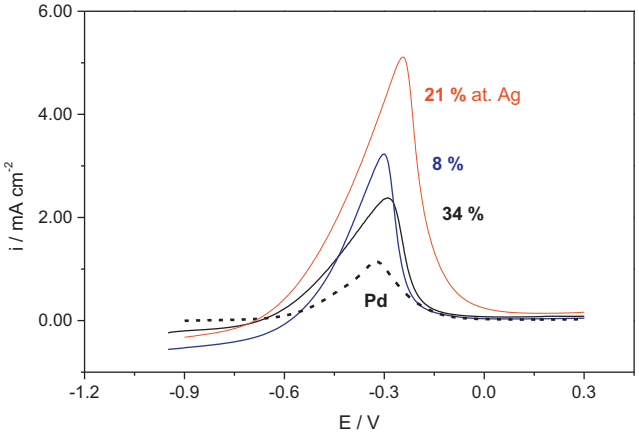

Fig. 5. Cyclic voltammograms in 1.0 M NaOH + 1.0 M EtOH solution of Pd–Ag alloy films (8, 21 and 34 at.% Ag) and Pd bulk. υ = 20 mV s^{-1}. The current was normalized to EASA.

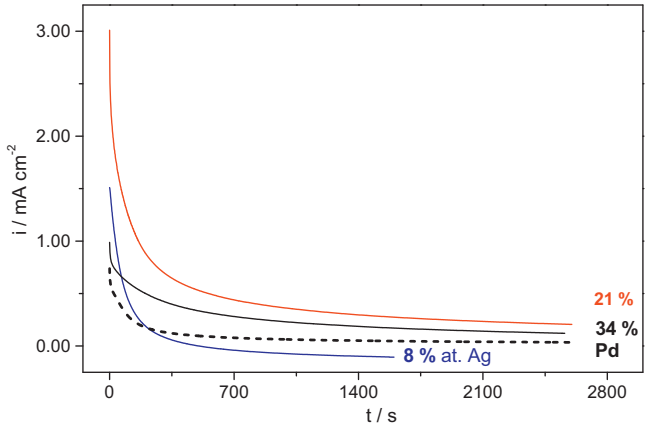

Fig. 6. Chronoamperometric curve for ethanol oxidation at −0.4 V on Pd–Ag alloys (8, 21 and 34 at.% Ag) and Pd bulk in 1.0 M NaOH + 1.0 M EtOH solution. The current was normalized to EASA.

poisoning, probably by intermediate species of the EOR. According to the literature, CH_3CO_{ads} intermediate is formed on the Pd catalyst in the alkaline medium, and its reaction with OH_{ads} is determining for the rate reaction [29]. We may then conclude that the less rich Ag alloy exhibits the lower ability towards the EOR due to its lower ability to promote the OH adsorption and consequently to desorb intermediate products formed on the EOR.

The overall results point out that the effect of alloying Ag atoms to Pd might play a role similar to that of alloying Ru atoms with Pt, providing oxygen-containing species needed to oxidize intermediate species, as advocated by the so called bifunctional mechanism.

3.4. Oxygen reduction reaction

Fig. 7 shows the typical linear voltammograms obtained in an O_2-saturated 1.0 M NaOH solution for the different Pd–Ag alloys and pure Pd. To compare their intrinsic catalytic activity towards the ORR, the current was normalized to EASA. Contrast-

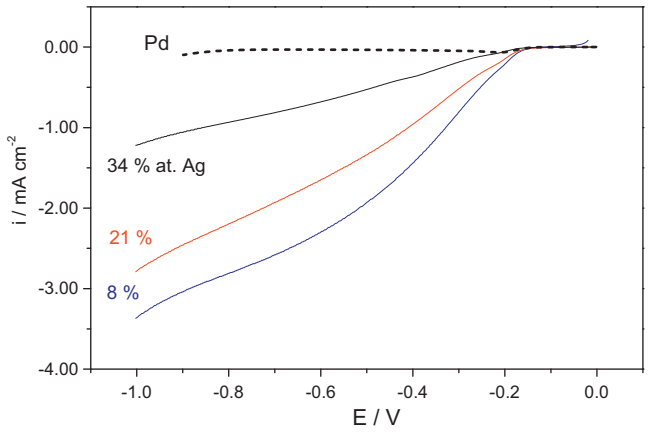

Fig. 7. Linear voltammograms for ORR on Pd–Ag alloys (8, 21 and 34 at.% Ag) and Pd bulk in 1.0 M NaOH solution. υ = 5 mV s^{-1}. The current was normalized to EASA.

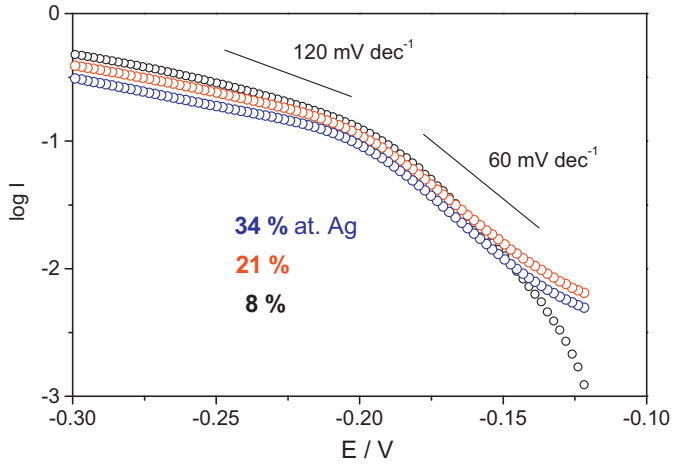

Fig. 8. Tafel plot for the ORR on Pd–Ag alloys and Pd bulk in 1.0 M NaOH solution.

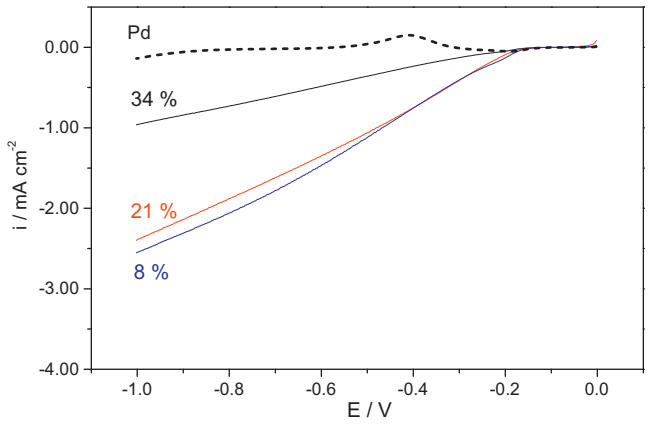

Fig. 9. Linear voltammograms for ORR on Pd–Ag alloys and Pd bulk in 1.0 M NaOH + 0.1 M EtOH solution at room temperature. $\upsilon = 5\,mV\,s^{-1}$. The current was normalized to EASA.

ing to Pd bulk, the polarization curves of the Pd–Ag alloys show a mixed control over the potential range cycled, not reaching a well defined diffusion-limited current density. All Pd–Ag alloys exhibit an enhanced ORR activity compared to pure Pd or pure Ag (not shown). The highest ORR current is observed for the alloy composition of 8 at.% Ag. The highest activity of this alloy is also confirmed from the results depicted from the Tafel slopes and the ORR current at a constant potential (Table 3). Since the lowest Ag content alloy exhibited the lowest ability for the OH adsorption and oxide formation, these results may point out that the ORR catalyst activity is inhibited by the OH adsorption. Such phenomenon is in agreement with the data obtained by other authors [15,27,30].

The current density on the 8 at.% Ag content alloy at −0.25 V, a potential within the kinetics controlled region (Table 3), resembles the value obtained at an equivalent potential by Jiang et al. for silver nanoparticles coated with Pd, which were also shown to be highly active [18]. Although silver has a promotion effect on the catalytic activity of Pd, the maximum ORR activity of Pd–Ag alloys was found at a very low percentage of Ag, in contrast to other alloying elements such as Co and Cu (40 at.%) [31]. A possible reason for this result comes from the higher stability of the adsorbed oxygen atom (resultant from O_2 splitting) on Co and Cu, compared to Ag, as predicted by the thermodynamic data [32]

Tafel plots for the ORR on Pd alloys, Fig. 8, reveal two Tafel slopes, a smaller one observed from −0.15 to −0.20 V (low overpotentials) and a higher one from −0.20 to −0.30 V (high overpotentials). Pd bulk also exhibits a transition from a low Tafel slope to a higher one, but in a more cathodic potential range. For the Pd–Ag alloys, the Tafel slope on the low overpotential region is close to 60 mV dec^{-1} (Table 3), resembling the literature data for Pd and Pt [33] and Pd coated Ag nanoparticles [18]. In the high overpotential region, the Tafel slope on Pd–Ag alloys deviates from the typical 120 mV dec^{-1}, usually reported in the literature for high overpotentials on Pd and others Pd alloys. This divergence may be due to mass transfer effects on the observed current in that potential range. Independently of the potential region, the lowest Tafel slope is observed on the 8 at.% Ag alloy, which is indicative of the better performance of this electrocatalyst on the ORR.

In order to investigate the activity of the Pd–Ag alloys towards ORR under ethanol crossover conditions, their voltammetric behavior towards ORR in the presence of ethanol was also investigated, Fig. 9. Contrasting to pure Pd, the results show a high ethanol tolerance, even though an increase in the overpotential under the same current density is observed in all alloys. For example, at 0.5 mA cm^{-2}, a cathodic shift of approximately 25, 75 and 125 mV is observed on the alloys containing 21%, 8% and 34 at.% Ag respectively. The increase in overpotential is probably due to ethanol and oxygen competition for adsorption on the same surface active sites. This behavior is also very similar with the electrochemical response observed on Pd coated Ag catalysts [18].

4. Conclusions

Pd–Ag alloys were successfully synthesized by means of sequential Ag and Pd electroless deposition on an oxidized/activated stainless steel substrate. It was demonstrated that Pd–Ag alloys can present a better catalytic activity towards the EOR, than Pd bulk, at room temperature. The highest catalytic activity for the EOR was exhibited by the 21 at.% Ag content alloy. The lowest Ag content alloy was found to be the most susceptible to surface poisoning by adsorbed intermediates on the EOR. Such phenomena were interpreted on basis of the bifunctional mechanism.

The Pd–Ag alloys under study, also revealed a higher ORR activity at room temperature, compared to Pd. The maximum activity for the ORR was observed at the alloy composition of 8 at.% Ag, which can be in part ascribed to the reduced OH coverage on this electrode material. In the presence of ethanol all Pd–Ag alloys showed a good ORR selectivity and activity, much superior to pure Pd.

While these studies revealed the promising potential of Pd–Ag alloy to be an effective catalyst for cathode or anode in ethanol direct fuel cells (DEFCs), its preparation as a nanomaterial dispersed on a carbon support remains a subject of research in the future.

Acknowledgments

The authors thank FCT (Portugal's Foundation for Science and Technology) for financial support through the CQ-VR Research Unit (POCTI-SFA-3-616).

Appendix A. Supplementary data

Supplementary data associated with this article can be found, in the online version, at doi:10.1016/j.jpowsour.2011.03.062.

References

[1] T.N. Danks, R.C. Slade, J.R. Varcoe, J. Mater. Chem. 13 (2003) 712.
[2] Z.X. Liang, T.S. Zhao, J.B. Xu, L.D. Zhu, Electrochim. Acta 54 (2009) 2203–2208.
[3] G. Cui, S. Song, P. Shen, A. Kowal, C. Bianchini, J. Phys. Chem. C 113 (2009) 15639–15642.
[4] C. Bianchini, P. Shen, Chem. Rev. 109 (2009) 4183–4206.
[5] L. Jiang, A. Hsu, D. Chu, R. Chena, J. Electrochem. Soc. 156 (2009) B370–B376.
[6] F. Lima, J. Zhang, M. Shao, K. Sasaki, M. Vukmirovic, E. Ticianelli, R. Adzic, J. Phys. Chem. C 111 (2007) 404–410.

[7] M. Nie, H. Tang, Z. Wei, S. Jiang, P. Shen, Electrochem. Commun. 9 (2007) 2375–2379.
[8] J. Lua, S. Lua, D. Wanga, M. Yanga, Z. Liub, C. Xub, S. Jianga, Electrochim. Acta 54 (2009) 5486–5491.
[9] Q. He, W. Chen, S. Mukerjee, S. i Chenmand, F. Laufek, J. Power Sources 187 (2009) 298–304.
[10] Y Wanga, T. Nguyena, X. Liub, X. Wanga, J. Power Sources 195 (2010) 2619–2622.
[11] S.Y. Shen, T.S. Zhao, J.B. Xu, Y.S. Li, J. Power Sources 195 (2010) 1001–1006.
[12] S Nguyen, H. Law, H. Nguyen, N. Kristian, S. Wang, S. Chan, X. Wang, Appl. Catal. B: Environ. 91 (2009) 507–515.
[13] O. Savadogo, K. Lee, K. Oishi, S. Mitsushima, N. Kamiya, K. Ota, Electrochem. Commun. 6 (2004) 105–109.
[14] B. Li, J. Prakash, Electrochem. Commun. 11 (2009) 1162.
[15] F. Gobal, R. Arab, J. Electroanal. Chem. 647 (2010) 66–73.
[16] M. Shao, K. Sasaki, R. Adzic, J. Am. Chem. Soc. 128 (2006) 3526–3527.
[17] J. Kim, J. Park, T. Momma, T. Osaka, Electrochim. Acta 54 (2009) 3412–3418.
[18] L. Jiang, A. Hsu, D. Chu, R. Chen, Electrochim. Acta 55 (2010) 4506.
[19] M. Ayturk, Y. Ma, J. Membr. Sci. 330 (2009) 233.
[20] Y. Ma, B. Akis, M. Ayturk, F. Guazzone, E. Engwall, I. Mardilovich, Ind. Eng. Chem. Res. 43 (2004) 2936.
[21] B. Nair, J. Choi, M. Harold, J. Membr. Sci. 288 (2007) 67.
[22] M.E. Ayturk, Y.H. Ma, J. Membr. Sci. 330 (2009) 233–245.
[23] J. Clavilier, R. Faure, G. Grimet, R. Durand, J. Electroanal. Chem. 107 (1980) 205.
[24] O.M. Løvvik, M. Susanne, Opalka, Surf. Sci. 602 (2008) 2840.
[25] C. Sonwane, J. Wilcox, Y. Ma, J. Chem. Phys. 125 (2006) 184714.
[26] A.N. Correia, L. Mascaro, S. Machado, L. Avaca, Electrochim. Acta 42 (1997) 493.
[27] F. Onana, S. Bath, O. Savadogo, J. Electroanal. Chem. 636 (2009) 1–9.
[28] G. Camara, R. Lima, T. Iwasita, Electrochem. Commun. 6 (2004) 812–815.
[29] Z. Liang, T. Zhao, J. Xu, L. Zhu, Electrochim. Acta 54 (2009) 2203.
[30] J. Zhang, Y. Mo, M. Vukimirovic, R. Klie, K. Sasaki, R. Adzic, J. Phys. Chem. B 108 (2004) 10955.
[31] K. Lee, O. Savadogo, A. Ishihara, S. Mitsushima, N. Kamiya, K. Ota, J. Electrochem. Soc. 153 (2006) B370–376.
[32] J. Fernandez, D. Walsh, A. Bard, J. Am. Chem. Soc. 127 (2005) 357–365.
[33] L. Jiang, A. Hsu, D. Chu, R. Chena, J. Electrochem. Soc. 156 (2009) B370.